Membrane permeability: characteristic times and lengths for oxygen, and a simulation-based test of the inhomogeneous solubility-diffusion model

Oriana De Vos,[†] Richard M. Venable,[‡] Tanja Van Hecke,[¶] Gerhard Hummer,[§] Richard W. Pastor,[‡] and An Ghysels[*,†]

†*Center for Molecular Modeling, Ghent University, Technologiepark 903, 9052 Gent, Belgium*

‡*Laboratory of Computational Biology, National Heart Lung Blood Institute, National Institutes of Health, Bethesda, Maryland, USA*

¶*Department of Information Technology, Ghent University, Belgium*

§*Department of Theoretical Biophysics, Max Planck Institute of Biophysics, 60438 Frankfurt am Main, Germany, and Institute for Biophysics, Goethe University Frankfurt, 60438 Frankfurt am Main, Germany*

E-mail: an.ghysels@ugent.be

Abstract

The balance of normal and radial (lateral) diffusion of oxygen in phospholipid membranes is critical for biological function. Based on the Smoluchowski equation for the inhomogeneous solubility-diffusion model, Bayesian analysis (BA) can be applied to molecular dynamics trajectories of oxygen to extract the free energy, and the normal and radial diffusion profiles. This paper derives a theoretical formalism to convert these profiles into characteristic times and lengths associated with entering, escaping, or completely crossing the membrane. The formalism computes mean first passage times and

holds for any process described by rate equations between discrete states. BA of simulations of eight model membranes with varying lipid composition and temperature indicate that oxygen travels 3 to 5 times further in the radial than in the normal direction when crossing the membrane in a time of 15 to 32 ns, thereby confirming the anisotropy of passive oxygen transport in membranes. Moreover, the preceding times and distances estimated from the BA are compared to the aggregate of 280 membrane exits explicitly observed in the trajectories. The comparison supports the BA approach and, therefore, the applicability of the Smoluchowski equation to membrane diffusion. Given the shorter trajectories required for the BA, these results validate the BA as a computationally attractive alternative to direct observation of exits when estimating characteristic times and radial distances. The effect of collective membrane undulations on the BA is also discussed.

I. Introduction

Diffusion of permeants through membranes has been studied for over 100 years. The efficiency of transport through membranes is expressed by the permeability P, which is the ratio $J/\Delta c$ of the flux of molecules over the concentration difference across the membrane in steady-state regime (Fig. 1a). Overton's observations established that the permeability of a solute is proportional to its solubility.[1] In more recent work, the permeability is frequently expressed as follows,[2–4]

$$\frac{1}{P} = e^{-\beta F_{\text{ref}}} \int_{-h/2}^{h/2} \frac{1}{D_{\perp}(z) e^{-\beta F(z)}} dz \tag{1}$$

where $\beta = 1/k_B T$ is the inverse temperature, h is the thickness of the membrane, $F(z)$ is the free energy profile for the permeant across the membrane, $D_{\perp}(z)$ is the permeant diffusion profile for diffusion normal ($\perp$) to the membrane plane, and F_{ref} is the reference free energy in the bulk water. This expression for P assumes that molecules diffuse in an inhomogeneous medium described by the Smoluchowski equation, also known as the inhomogeneous solubility diffusion model.[3] The permeability in Eq. 1 follows from solving the Smoluchowski

equation in steady-state regime under the boundary condition of constant concentration difference.[2] While the ratio of flux and concentration difference can, in principle, be calculated directly from non-equilibrium simulations (Fig. 1a), use of Eq. 1 assumes the validity of a diffusion model.

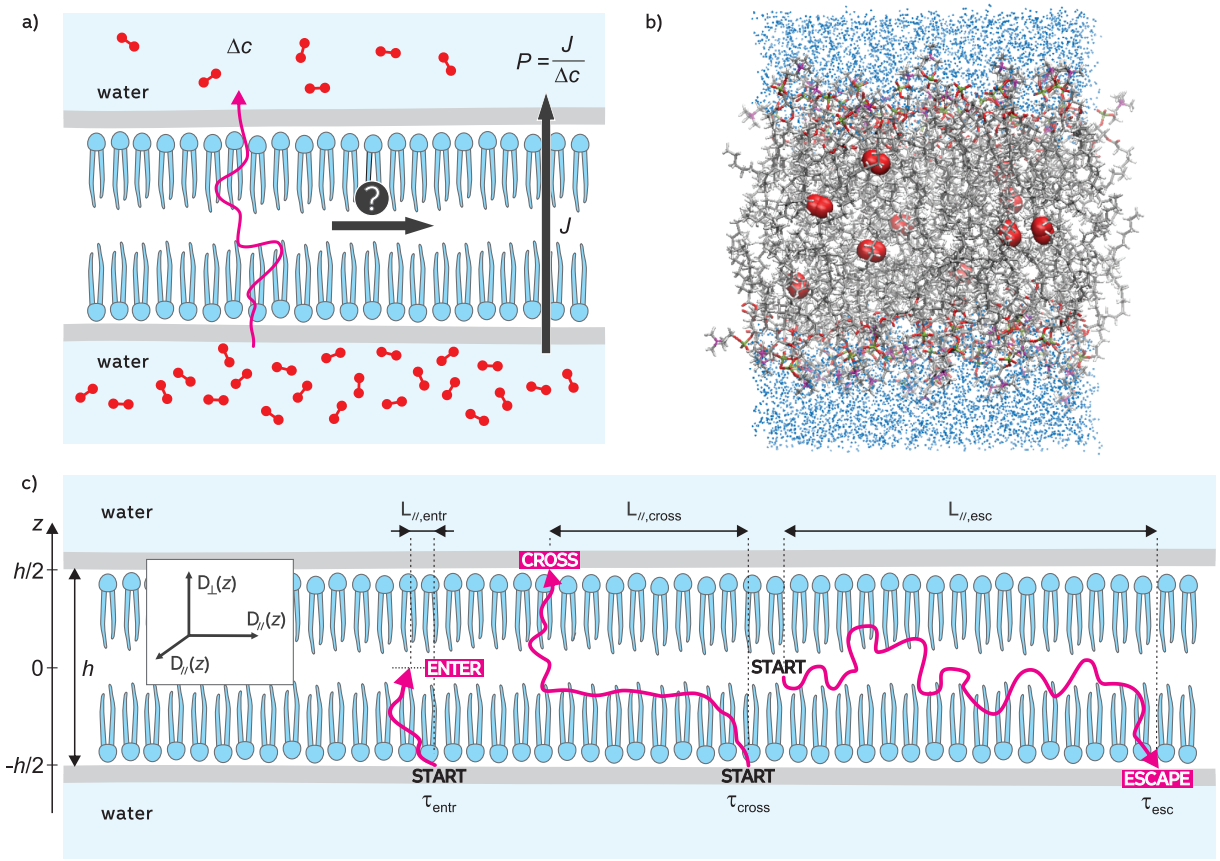

Figure 1: (a) Definition of permeability P as ratio of flux and concentration difference. P does not give information on radial transport. (b) Simulation box with 72 DOPC lipids, 10 O_2 molecules (red) and 2409 water molecules (blue). DOPC C-atoms are grey, H-atoms white, O-atoms red, the P-atom green and the N-atom magenta. (c) Membrane of thickness h with normal diffusion $D_\perp$ and radial diffusion $D_{||}$ profiles. The membrane center is located at $z = 0$. Schematic trajectories (red) are used to illustrate the crossing time τ_{cross}, escape time τ_{esc}, and entrance time τ_{entr}, during which oxygen travels over radial distances $L_{||}$.

The radial component of the diffusion tensor, $D_{||}$, is conspicuously absent from Eq. 1. Hence, this equation provides no information on how far a permeant travels in the membrane before it exits. In recent work (herein referred to as Ref. 5), the authors solved the Smolu-

chowski equation for a layered medium, such as the bilayer membrane, using separation of variables into radial (r) and normal (z) coordinates, and splitting the equation into radial and normal equations. This approach allowed the computation of the so-called propagator $p(z, r, t|z_0)$, which is the oxygen concentration at time t at depth z and a radial distance r from the reference, given that the molecule started at $z = z_0$ at $t = 0$. The fact that this propagator p contains both the $D_\perp$ and $D_{||}$ profiles will be exploited in the present paper. The propagator will be used to predict not only the permeability for normal transport across the membrane, but also the radial diffusion within the membrane.

A central question for oxygen transport is the balance between normal and radial transport. For instance, if the normal flux is low and the radial flux is high, the permeant has ample time to explore the membrane interior, which may be related to biological function. One indication of the radial/normal balance is the anisotropy ratio, $D_{||}/D_\perp$. Normal diffusion is somewhat faster than radial diffusion in the tail region, where oxygen easily moves in the direction of the tails. In the center of the membrane, oxygen moves more easily parallel to the membrane. However, the free energy $F(z)$ is typically a more effective modulator of transport than the diffusion anisotropy. This was investigated using a 5-compartmental model, where the free energy barrier in the head group region was shown to have a large effect.[5] The barrier is absent in a simple membrane model consisting of a pure hexadecane slab immersed in water, making this system an inadequate model for biological membrane permeation. Likewise, the 1-compartmental model implied by the Meyer-Overton rule lacks the important features of the free energy and can only provide a semi-quantitative estimate of the permeability.

In this paper, we will quantitate the balance between normal and radial transport by assessing characteristic times and lengths illustrated in Fig. 1c. The escape time τ_{esc} is the time required for an oxygen molecule to leave the center of the membrane and to exit above or below. The radial distance $L_{||,\text{esc}}$ is the distance on average traveled by an oxygen molecule before exiting the membrane. The comparison of $L_{||,\text{esc}}$ with half the membrane

thickness $h/2$ is therefore another measure of the anisotropy. Other characteristic times are the entrance time τ_{entr}, defined as the average time needed to reach the membrane center starting from its surface, and the crossing time τ_{cross}, defined as the average time needed to cross the membrane entirely (Fig. 1c). A first important contribution of the paper is the theoretical derivation of expressions for τ and $L_{||}$ using the propagator p associated with the Smoluchowski equation.

Recently, inspired by anomalous diffusion traits encountered in biology, the applicability of the Smoluchowski equation (and thereby Eq. 1) to membrane diffusion has been questioned, and the use of more advanced models has been promoted.[6,7] For pure diffusion, the mean square distance grows linearly in Brownian processes with a Gaussian step distribution. Anomalous diffusion can be recognized by a non-linear scaling of the MSD. A large variety of models exist to model this non-universal behavior,[8–10] such as time-fluctuating non-stationary diffusivities,[11] diffusing diffusivities,[12,13] accelerating subdiffusion,[14] non-gaussian step distributions,[15] Levy flight models,[16] fractional Langevin equations,[17] fractional Brownian motion,[18] or generalized Langevin equation motion.[18,19] Chipot and Comer proposed the time-fractional Smoluchowski equation for diffusion in an inhomogeneous medium,[6] and Hinsen and Kneller implemented a Bayesian analysis of anomalous lateral lipid diffusion related to fractional Brownian motion (FBM).[20]

The question arrises whether the essentials of oxygen transport can be captured by the Smoluchowski equation without resorting to such advanced mathematical approaches. The preceding times and lengths based on the Bayesian analysis (BA) approach are very relevant properties for understanding oxygen transport, and they are natural targets for the validation. Here the τ and $L_{||}$ from BA are compared with those exits explicitly observed in extended simulated trajectories from molecular dynamics (MD) simulations, thereby providing a direct test of the BA approach and, on a more fundamental level, the Smoluchowski equation itself. The statistics of escape times are notoriously bad, and the aggregate of the seven studied systems giving 280 observed exits was needed to study the accuracy of the

BA approach. Another potentially confounding issue is membrane undulations, which blur the registration of membrane exits. To explore the effect of undulations, τ and $L_{||}$ were also determined in a larger simulation box. The test of the Smoluchowski equation by comparing escape times and lengths is the second important contribution of this paper. It is based on MD simulations of oxygen in 4 different lipid bilayers at various temperatures, giving 8 modeled systems.

The Theory and Methods section starts with a review how the position dependent diffusion tensors and free energies are extracted from the trajectories using Bayesian analysis based on the Smoluchowski equation as developed in Ref. 5. After this review, we present a new methodology for predicting the averages of characteristic times and distances analytically from the diffusion and free energy profiles. The derivation of the equations for τ and $L_{||}$ with various absorbing boundary conditions is the main theoretical contribution of the paper. The formulation for mean first passage times for membranes is in fact generally applicable and holds for any process described by rate equations between discrete states. The traveled radial distance, which has a more elaborate two-dimensional distribution, has been treated with the same formalism.

In the Results and Discussion section, the simulation protocol and theoretical formulations are first applied to seven modeled systems, showing the effect of lipid composition and temperature on P, τ, and $L_{||}$. The connection between permeabilities, τ and $L_{||}$ is discussed, and it is shown that each property gives additional insight in the transport process. The properties τ_{esc} and $L_{||,\text{esc}}$ are used to validate the diffusive assumption implied by the Smoluchowski equation by comparing them with directly observed oxygen escapes. A statistical analysis is provided to assess the significance of this comparison. An eighth system is presented with a four times larger unit cell box to investigate the possible effect of membrane undulations on these properties. The Conclusion section summarizes the work.

II. Theory and methods

A. Review: Smoluchowski equation and Bayesian analysis

1. The propagator in a membrane

This subsection reviews the methodology of Ref. 5. The assumed underlying model is diffusion on a free energy profile $F(z)$ with a position and orientation dependent diffusivity tensor. The diffusion normal to the membrane is characterized by $D_\perp(z)$ and parallel to the membrane by $D_{||}(z)$; both depend on the location z along the normal of the membrane (see Fig. 1c). The aim is to construct the propagator $p(r, z, t|z_0)$, which describes the probability of finding the oxygen molecule at location z in the membrane at time t, assuming it started at location z_0 at time 0 and traveled a radial distance r parallel to the plane with respect to its original xy location. The propagator can be used to compute characteristic times and lengths. The radial dependence of the propagator on r is a prerequisite for estimating the mean traveled radial distance.

The evolution of $p(r, z, t|z_0)$ is described by the Smoluchowski equation. Ref. 5 showed that the Smoluchowski equation in a layered system like a membrane, an inhomogeneous system with translational invariance in the xy-plane, splits into two equations using separation of the variables z and r, one for normal diffusion along the z axis and one for radial diffusion in the plane. The radial diffusion is a textbook example and is described by Bessel functions J_n of the first kind and nth order. The normal diffusion reduces to one-dimensional diffusion on $F(z)$

$$\frac{\partial Q}{\partial t} = \frac{\partial}{\partial z}\left(D(z) e^{-\beta F(z)} \frac{\partial}{\partial z}\left(e^{\beta F(z)} Q \right) \right). \tag{2}$$

$Q(z,t)\,dz$ is the probability of finding an oxygen molecule in a layer $[z, z+dz]$ of the membrane at time t. To determine the F, $D_\perp$, and $D_{||}$ profiles from the simulations later on, the z-axis is discretized in bins $\{i\}$, giving the free energy F_i in bin i, the normal diffusion $D_{\perp,i+1/2}$ between bins i and $i+1$, and the radial diffusion $D_{||,i}$ in layer i. The discretized version of

the normal equation features the rate matrix R, that describes the transition rates between neighboring bins,

$$\frac{dQ(i,t)}{dt} = \sum_j R_{ij} Q(j,t) \tag{3}$$

where $Q(i,t)$ is now the probability to be in bin i at time t. The rate matrix is constructed from the discretized F_i and $D_{i+1/2}$ profiles and is a tridiagonal matrix with adapted corner elements to account for periodicity.[21] By solving this equation under the initial condition of the oxygen molecule being in a particular bin j at time 0, i.e. $Q(i,0) = \delta_{ik}$, the propagator for normal diffusion is readily found as the matrix exponential of Rt,

$$Q(i,t|j) = [e^{Rt}]_{ij}. \tag{4}$$

We now return to the original question of the probability $p(r,z,t|z_0)$, where normal and radial diffusion are combined. After discretization of both z (bins i) and the radial distance r (bins m, width Δr), the discretized propagator for diffusion in layered system, is given by[5]

$$\tilde{p}(i,m,t|j) = \Delta r \sum_{\alpha_k} 2r_m \frac{J_0(\alpha_k r_m)}{s^2 J_1^2(x_k)} \left[e^{Rt - \alpha_k^2 \mathcal{D} t}\right]_{ij} \tag{5}$$

where $\tilde{p}$ is the probability for the oxygen to be in z-bin i and r-bin m at time t, when it was in z-bin j at the origin at time 0. This propagator describes two-dimensional diffusion (radial and normal). It features an adapted matrix exponential that accounts for diffusion parallel into the layers of the membrane. The variable s is a large radial distance, where the probability can safely be assumed to have died to zero. The summation is over the zeros $x_k = s\,\alpha_k$ of the J_0 Bessel function which are tabulated in, e.g., the scipy package of python, and the summation is in practice truncated when convergence is reached. The matrix $\mathcal{D}$ is diagonal with the discretized parallel diffusion profile $D_{||,i}$ on its diagonal. As could be expected, the propagator $\tilde{p}$ in a membrane depends both on R – which is constructed from the free energy and normal diffusion profile – and the parallel diffusion profile. Once the

profiles are determined, we will use the propagator in Eq. 5 to investigate the characteristic length and times of oxygen transport in the membrane.

2. Extracting free energy and diffusion profiles

The free energy $F(z)$ and normal diffusion profile $D_\perp(z)$ were determined from MD simulations previously by several groups using various techniques, such as measuring force correlations in constrained simulations,[2] a Bayesian approach,[5,21,22] local mean first passage times,[23] or velocity and position autocorrelation functions.[24] In a few cases, $D_{||}$ profiles were also published using similar techniques for water and ion transport.[2,25–27]

In this paper, the extraction of the F, $D_\perp$ and $D_{||}$ profiles from the MD trajectories is based on Bayesian analysis. The theoretical propagators in Eqs. 4 and 5 are matched with the observed propagation of oxygen molecules in the trajectories by randomly varying the profiles in a Monte Carlo routine. The likelihood of observing the MD trajectories, given the profiles, is computed at each Monte Carlo step. The result of the routine is a distribution of profiles around the most likely profiles, and the reported profiles in this work are the average profiles of these distributions.

To account for the short time scale behavior of oxygen in membranes, the Bayesian analysis was repeated for several lag times between 20 and 50 ps, and the final profiles were obtained by a fit towards infinitely long time scales. The example of DOPC/298 is plotted in Fig. 2; other profiles are reported in Ref. 22 where the effect of disorder in the lipid chains due to unsaturation on oxygen diffusion is discussed.

B. Expressions for characteristic times and lengths

1. Mean first passage time

The computation of characteristic times for a membrane slab falls into two categories from a methodological point of view. One category covers the characteristic times for leaving the slab on either side, i.e. the top or the bottom side of the slab. The escape time τ_{esc} from the

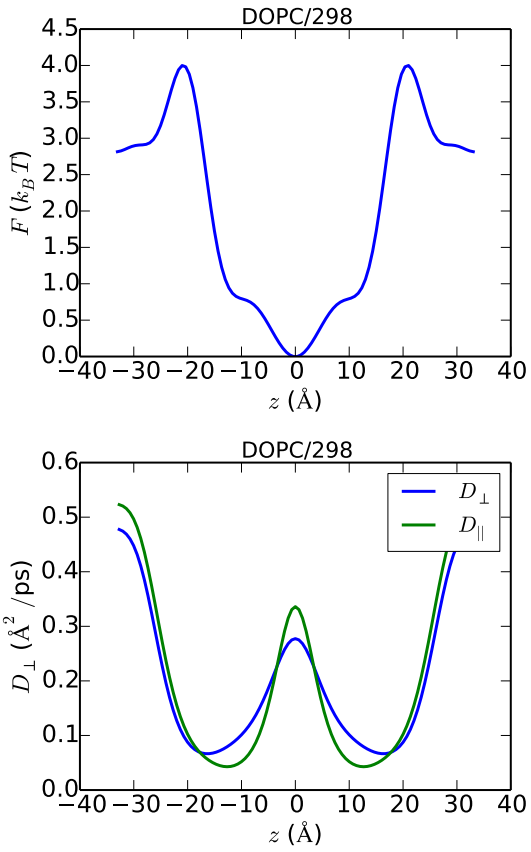

Figure 2: Profiles F, $D_\perp$ and $D_{||}$ of DOPC/298 obtained from Bayesian analysis of the MD trajectories.

membrane center to the water phase belongs to this category. The other category covers the characteristic times for transiting from one side to the other side of a slab. For instance, the entrance time τ_{entr} is the transit through half the membrane, and the crossing time τ_{cross} is the crossing through the entire membrane.

First, we derive an equation for the time needed to leave a slab on either side. The starting point is the one-dimensional Smoluchowski equation (Eq. 2) for a membrane with absorbing boundary conditions on both sides of the slab.[28,29] When an oxygen molecule arrives, it is absorbed in the water phase and never returns to the membrane slab. This means that the computed escape time τ_{esc} is actually a mean first passage time through the membrane surfaces. Our derivation in the following can be applied to more general problems of first passage times, where one has non-absorbing bins and absorbing bins. To illustrate

the general applicability of our derivation, the notation is made more general.

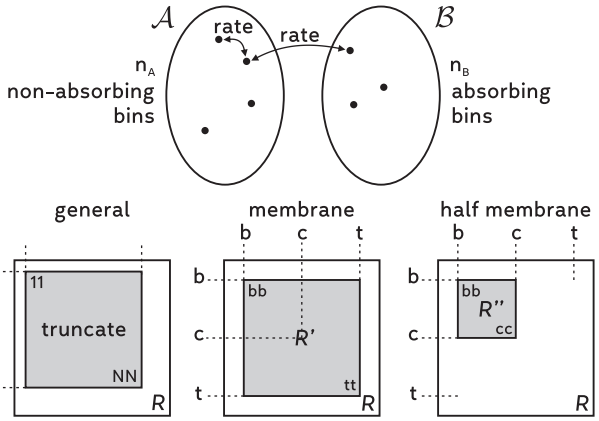

Figure 3: (Upper panel) The n_A non-absorbing states $\in \mathcal{A}$ and n_B absorbing states $\in \mathcal{B}$ are connected by rate matrix elements R_{ij}. (Lower panel) Truncation of rate matrix covering bins 1 to N, in the general case. For the characteristic times and lengths in this work, R is truncated to R' for the full membrane covering bins from bottom (b) to top (t), by removing the water bins, and to R'' for the half membrane covering bins from bottom (b) to center (c).

Let $\mathcal{A}$ be the set of n_A non-absorbing bins, and $\mathcal{B}$ the set of n_B absorbing bins. The rate matrix R describes the transitions between all possible bins and has size $(n_A{+}n_B){\times}(n_A{+}n_B)$, as shown in Fig. 3. Assume the matrix R' describes the transitions between non-absorbing bins only, here the bins within the membrane slab. Then R' is a truncated rate matrix, i.e. the $n_A \times n_A$ matrix submatrix obtained by barring n_B rows and columns from R. The elements are given by $R'_{ij} = R_{ij}, \forall i,j \in \mathcal{A}$. Assume that the initial position of the particle is a delta peak at bin $k \in \mathcal{A}$, and the propagator is given by $[e^{R't}]_{ik}$ as in Eq. 4, featuring the truncated rate matrix R'. The probability G that the particle is still present in the slab after some lag time t is the spatial integral of the propagator over the slab, which can be replaced by a summation over the bins in the slab,

$$G(t|k) = \sum_{i \in \mathcal{A}} \left(e^{R't} \right)_{ik} . \tag{6}$$

The probability distribution $\rho(t|k)$ to exit the slab at some time t relates to the time deriva-

tive of G,

$$\rho(t|k) = -\frac{\partial G(t|k)}{\partial t} = -\sum_{i\in\mathcal{A}} \left(R' e^{R't}\right)_{ik}. \tag{7}$$

The distribution ρ is used to calculate the mean time $\tau(k)$ that a particle remains in the slab, assuming its initial position was bin k at time 0,

$$\tau(k) = \int_0^\infty t\rho(t|k)dt. \tag{8}$$

Since ρ dies to zero at long times because of the absorbing bins, the mean time can be converted using partial integration to a time integral of G,

$$\tau(k) = -\int_0^\infty G(t|k)dt. \tag{9}$$

The adapted rate matrix R' only has negative eigenvalues because all probability flows out of the slab as time increases. The time integral in Eq. 6 can therefore be evaluated explicitly as

$$\tau(k) = \sum_{i\in\mathcal{A}} \int_0^\infty \left(e^{R't}\right)_{ik} dt = -\sum_{i\in\mathcal{A}} \left(R'^{-1}\right)_{ik} \tag{10}$$

where R'^{-1} is the inverse matrix of R'.

Second, we derive an equation for the time needed to transit from one side to the other side of the slab. We are interested in particles that start their trajectory on one side of the slab and have their first exit from the slab at the other side. The above reasoning then needs an adaptation to take into account the condition of 'leaving from one particular side'. The key relation to achieve the adaptation, is to use the conservation of probability for any non-absorbing bin $l \in \mathcal{A}$. The total flux from bin l to all other bins, be it in $\mathcal{A}$ or in $\mathcal{B}$, is zero,

$$\sum_{i\in\mathcal{A}} R'_{il} + \sum_{j\in\mathcal{B}} R_{jl} = 0, \quad \forall l \in \mathcal{A}. \tag{11}$$

The probability distribution $\rho(t|k)$ in Eq. 7 is rewritten using this conservation law,

$$\begin{aligned} \rho(t|k) &= -\sum_{i\in\mathcal{A}}\sum_{l\in\mathcal{A}} R'_{il}\left(e^{R't}\right)_{lk} && (12)\\ &= \sum_{j\in\mathcal{B}}\sum_{l\in\mathcal{A}} R_{jl}\left(e^{R't}\right)_{lk} = \sum_{j\in\mathcal{B}}\rho_j(t|k) && (13)\end{aligned}$$

which shows that ρ is the sum of fluxes out of the slab into the individual j absorbing states, where each flux ρ_j is given by

$$\rho_j(t|k) = \sum_{l\in\mathcal{A}} R_{jl}\left(e^{R't}\right)_{lk}. \quad (14)$$

This equation means that the flux to the absorbing bin j is equal to the probability in the non-absorbing bins ($\left(e^{R't}\right)_{lk}$), multiplied by the rate to exit from l to that particular bin j (R_{jl}). The total probability to exit from $\mathcal{A}$ to bin j is obtained by integrating ρ_j over time,

$$P_j(k) = \int_0^\infty \rho_j(t|k)dt = -\sum_{l\in\mathcal{A}} R_{jl}\left(R'^{-1}\right)_{lk}. \quad (15)$$

This allows us to construct the ratio ρ_j/P_j, which is the normalized probability distribution to exit through bin j after a lag time t. The mean time to exit through bin j is then obtained by taking the average,

$$\tau_{\to j}(k) = \int_0^\infty t\ \frac{\rho_j(t|k)}{P_j(k)}dt. \quad (16)$$

After partial integration of Eq. 16, using 14, and using the assumption that ρ dies off to zero for long times, we find the general expression for the mean time $\tau_{\to j}(k)$ to leave the slab to the absorbing bin j,

$$\tau_{\to j}(k) = \frac{\sum_{l\in\mathcal{A}} R_{jl}\left(R'^{-2}\right)_{lk}}{\sum_{l\in\mathcal{A}} R_{jl}\left(R'^{-1}\right)_{lk}}. \quad (17)$$

Equations 10 and 17 are the main formulas for the characteristic times in this paper. The equations for the mean first passage times apply to general rate problems consisting of non-absorbing and absorbing bins. Let us now work out the special case of a membrane slab

and assuming the Smoluchowski equation. The equations used in this work are summarized in Table 1, and the bins of the truncated rate matrices R' and R'' are shown in Figure 3. (1) The escape time τ_{esc} is obtained by setting the initial bin k at the center of the membrane $k = k_{\text{cent}}$ (bin c) in Eq. 10. The truncated rate matrix R' contains the bins from the membrane bottom to the top at $z = \pm h/2$ (bin b to bin t), and the absorbing bins are in the water phase (bin $b-1$, bin $t+1$). (2) For the crossing time τ_{cross}, the initial bin k is the bottom bin at $z = -h/2$ (bin b) in Eq. 17, and the j bin is the absorbing top bin at $z = h/2$ (bin $t+1$). The matrices R and R' are tridiagonal. Consequently, the summations $l \in \mathcal{A}$ in Eq. 17 are reduced to a single term only, $R_{N+1,N}$, which nicely drops out. (3) For the entrance time τ_{entr}, only half a membrane slab is considered, and the truncated rate matrix R'' covers only the bins between the membrane bottom at $z = -h/2$ and center at $z = 0$ (bin b to bin c). The absorbing bins are in the water phase and in the center (bin $b-1$ and $c+1$). The initial bin k is the bottom (bin b).

As a last case, the initial condition is not assumed to be a single peak in bin k, but the equilibrium distribution over the entire slab. The contributions $\tau(k)$ are then weighted by the equilibrium distribution $e^{-\beta F_k}$,

$$\tau_{\text{res}} = \frac{\sum_{k\in\mathcal{A}} \tau(k) e^{-\beta F_k}}{\sum_{k\in\mathcal{A}} e^{-\beta F_k}}. \tag{18}$$

This time τ_{res} can be interpreted as the average residence time of a particle in the slab under equilibrium conditions before exiting on either side.

2. Traveled radial distance

During the time spent in the membrane, the permeant will have traveled over some radial distance. For each characteristic time of the previous subsection, we will derive the associated mean traveled radial distances $L_{||}$ (see Fig. 1c). As for the mean times, the average distance depends on which fluxes (top and/or bottom) are taken into account.

Table 1: Derived equations for characteristic times and lengths. [a]

Eq.	time	Eq.	length
10	$\tau_{\rm esc} = -\sum_{i=b}^{t} \left(R'^{-1}\right)_{ic}$	28	$L^2_{\parallel,\rm esc} = \sum_m r_m^2 \sum_{\alpha_{k'}} A_{k'}(r_m) \left(R_{b-1,b}\left[(R' - \mathcal{D}'\alpha_{k'}^2)^{-1}\right]_{bc} + R_{t+1,t}\left[(R' - \mathcal{D}'\alpha_{k'}^2)^{-1}\right]_{tc}\right)$
17	$\tau_{\rm cross} = \frac{(R'^{-2})_{tb}}{(R'^{-1})_{tb}}$	25	$L^2_{\parallel,\rm cross} = \sum_m r_m^2 \sum_{\alpha_{k'}} A_{k'}(r_m) \frac{[(R' - \mathcal{D}'\alpha_{k'}^2)^{-1}]_{tb}}{(R'^{-1})_{tb}}$
17	$\tau_{\rm entr} = \frac{(R''^{-2})_{cb}}{(R''^{-1})_{cb}}$	25	$L^2_{\parallel,\rm entr} = \sum_m r_m^2 \sum_{\alpha_{k'}} A_{k'}(r_m) \frac{[(R'' - \mathcal{D}''\alpha_{k'}^2)^{-1}]_{cb}}{(R''^{-1})_{cb}}$

[a] Definitions are in Fig. 1c. The bin indices b, c, and t refer to the bottom, center, and top of the membrane, respectively.

The evaluation of $L_{||}$ requires the distribution of traveled distances when first passing the border of the membrane slab. Therefore, the derivation starts with constructing the flux through a radial bin in the mathematical framework of the previous subsection. The absorbing bins $j \in \mathcal{B}$ are the top or the bottom of the slab, which are numbered as $j = 0$ and $j = N + 1$ in this subsection for clarity. The slab consists of N bins. The radial bins are labeled by the index m, and r_m is the center of the m'th bin. The initial condition is a peak distribution in z-bin k at time $t = 0$ and location $r = 0$. The rate matrix for the slab is again the truncated rate matrix R'. All its eigenvalues are negative, and the total probability in the slab is hence not conserved. The probability to be in radial bin m near the bottom border (z-bin N), is given by the propagator $\tilde{p}(N, m, t)$, where R' is used in Eq. 5 instead of R. The flux in bin m through the bottom border is obtained by multiplying the propagator with the rate outwards of the border, $R_{j,N} = R_{N+1,N}$. A similar reasoning holds for the top border, where the propagator is $\tilde{p}(1, m, t|k)$ and the rate outwards is $R_{0,1}$. The

flux at time t through bin m at the top or bottom border of the slab becomes, respectively,

$$\rho_{\rm top}(r_m, t|k) = R_{0,1}\, \tilde{p}(1, m, t|k), \tag{19}$$

$$\rho_{\rm bot}(r_m, t|k) = R_{N+1,N}\, \tilde{p}(N, m, t|k). \tag{20}$$

These equations can also be cast into the formulation of Eq. 14 by rewriting the non-absorbing set $\mathcal{A}$ and absorbing set $\mathcal{B}$ to include radial "states", and realizing that flux between states is only allowed between neighboring states because of the tridiagonality of R'.

We first consider the flux through the bottom border only. This means that the mean radial distance will be taken over those particles that exit at the bottom of the slab, excluding those that exited through the top border before having crossed the bottom. The total flux through bin m at the bottom border is the time integral of $\rho_{\rm top}(r_m, t|k)$. Since the absorbing bins make the propagator die off to zero at long times, the total flux through m may be evaluated directly from Eq. 5 and Eq. 19,

$$\rho_{\rm bot}(r_m|k) = \int_0^\infty \rho_{\rm bot}(r_m, t|k)\, dt \tag{21}$$

$$= -R_{N+1,N} \sum_{\alpha_{k'}} A_{k'}(r_m) \left[(R' - \mathcal{D}'\alpha_{k'}^2)^{-1}\right]_{Nk} \tag{22}$$

where the shorthand notation

$$A_{k'}(r) = \Delta r\, 2r \frac{J_0(\alpha_{k'} r)}{s^2 J_1^2(x_{k'})} \tag{23}$$

is introduced, and $\mathcal{D}'$ is the truncated version of the diagonal matrix $\mathcal{D}$, matching the size of R'.

In the final step, the flux is normalized. $P_{\rm bot}(k)$ is the probability to exit at the bottom border (independent of time and radial bins) and is given by Eq. 15 with $j = N + 1$,

$$P_{\rm bot}(k) = -R_{N+1,N} \left(R'^{-1}\right)_{Nk}, \tag{24}$$

or alternatively, $P_{\rm bot}(k) = \sum_m \rho_{\rm bot}(r_m|k)$ when the number of Bessel functions is high and s is large in Eq. 22. The ratio $\rho_{\rm bot}(r_m|k)/P_{\rm bot}(k)$ is the normalized probability to exit through bin m, only considering the bottom border. The normalization means that only trajectories exiting through the bottom border are considered. This normalized distribution is used to calculate the mean traveled radial distance $L_{||}$ by taking the weighted average of r_m^2

$$L^2_{||,\rm bot}(k) = \sum_m r_m^2 \frac{\rho_{\rm bot}(r_m|k)}{P_{\rm bot}(k)}. \tag{25}$$

This expression is appropriate when considering trajectories that transit from one side to the other. A similar reasoning holds for exits through the top border, with similar quantities $\rho_{\rm top}(r_m|k)$, $P_{\rm top}(k)$, and $L^2_{||,\rm top}$.

Next, we consider the flux through bin m including both the top and bottom border,

$$\rho(r_m, t|k) \;\; = \;\; \rho_{\rm top}(r_m, t|k) + \rho_{\rm bot}(r_m, t|k). \tag{26}$$

The total flux through bin m is obtained by the time integral and yields,

$$\rho(r_m|k) = \rho_{\rm top}(r_m|k) + \rho_{\rm bot}(r_m|k). \tag{27}$$

All molecules exit with certainty either through the top or bottom border because of absorbing boundaries, such that $P_{\rm top}(k) + P_{\rm bot}(k) = 1$, and normalization is not necessary. The mean traveled radial distance $L_{||}$ is obtained by taking the weighted average of r_m^2

$$L^2_{||,\rm top/bot}(k) = \sum_m r_m^2 \; \left(\rho_{\rm top}(r_m|k) + \rho_{\rm bot}(r_m|k)\right). \tag{28}$$

This expression is appropriate when considering trajectories that escape from the membrane on either side.

Equations 25 and 28 are the main theoretical formulas for characteristic lengths in this

paper. A summary of the equations used in this work is given in Table 1. The initial bin k is chosen at the membrane bottom or center. For $L^2_{||,\mathrm{esc}}$ and $L^2_{||,\mathrm{cross}}$, the truncation covers the membrane bins. For $L^2_{||,\mathrm{entr}}$, only half of the membrane is considered, and $\mathcal{D}''$ denotes the truncated $\mathcal{D}$ matrix with the same size as R''. In this work, the root of the mean squared distances, $L_{||}$, is reported. Error bars on the mean squared distances are also converted by simply taking the root. The summations over the radial m-bins can also be evaluated analytically using properties of Bessel functions, as shown in the Supp. Info., but the numerical effect is negligible.

C. Simulation details

Eight membrane systems with varying composition and temperature are modeled using the CHARMM36 force field[30,31] and the CHARMM program.[32] Four membrane compositions are considered: 1-palmitoyl-2-oleoyl-sn-glycero-3-phosphocholine (POPC), 1,2-dioleoyl-sn-glycero-3-phosphocholine (DOPC), 1,2-dipalmitoyl-sn-glycero-3-phosphocholine (DPPC), and a model membrane representing the inner mitochondrial membrane (referred to as MITO) which was used in Ref. 5. The membranes are simulated at various temperatures. For instance, MITO is modeled at body temperature, while DPPC is modeled at a higher temperature where it is in the liquid phase.

The composition and temperatures of the eight bilayers simulated are listed in Table 2. Seven of these systems each contained 72 lipids and 10 O_2. The same protocol was followed as in Ref. 5. Four different initial conditions were generated, and the four replicates were simulated in the NVT ensemble (box sizes available in Supp. Info.) for 50 ns each, yielding 200 ns of data. The 8th system is four times larger containing 288 DOPC lipids and 40 O_2 (DOPC/298/lg in Table 2). The box is approximately doubled in size in the x and y-direction while maintaining the same water layer thickness. One replicate was simulated for 50 ns. The F and D profiles were generated with these MD trajectories using the same BA settings as in Refs. 5- 22, such as the definition of the basis functions, the number of Bessel

functions, the number of z-bins and r-bins, step size, number of equilibration steps and number of production steps in the Monte Carlo routine. An exception is the computation of $L_{||}$, where the number of Bessel functions and r-bins was varied until numerical convergence was achieved.

Table 2: Modeled systems.[a]

system	temp.	composition
POPC/310	310 K	72 POPC, 2242 water, 10 O_2
POPC/323	323 K	72 POPC, 2242 water, 10 O_2
DOPC/298	298 K	72 DOPC, 2409 water, 10 O_2
DOPC/310	310 K	72 DOPC, 2409 water, 10 O_2
DOPC/323	323 K	72 DOPC, 2409 water, 10 O_2
DPPC/323	323 K	72 DPPC, 2189 water, 10 O_2
MITO/310	310 K	72 lipids, 2890 water, 32 K^+, 8 Cl^-, 10 O_2
DOPC/298/lg	298 K	288 DOPC, 9636 water, 40 O_2

[a] The lipid composition in system MITO/310 includes cardiolipin and is specified in Ref. 5. The abbreviation 'lg' refers to the larger box size.

In order to compare the characteristic times and lengths based on free energy and diffusion profiles (BA) with direct observations of oxygen escaping from the membrane center (TRAJ), the trajectories were extended until all 10 O_2 had at least one exit (90% typically exited by 50 ns, though one system required 297 ns). The time difference and the traveled radial distance are stored between the time an oxygen molecule is first located in the center (here taken to be $|z| < z_{\mathrm{cent}}$) and when it first crosses the surface of the membrane ($|z| > z_{\mathrm{cut}}$). We used $z_{\mathrm{cent}} = 5$ Å and $z_{\mathrm{cut}} = h/2$ for an escape from the membrane of thickness h. Next, the average over all oxygen molecules and replicates (40 observations) is taken to compute the mean escape time $\tau_{\mathrm{esc}}^{\mathrm{TRAJ}}$ and mean squared traveled distance $L_{||,\mathrm{esc}}^{2,\mathrm{TRAJ}}$ as observed in the trajectories. In addition, the escapes from a series of other slab thicknesses were obtained by varying z_{cut}, giving the $\tau_{\mathrm{esc}}(z_{\mathrm{cut}})$ and $L_{||,\mathrm{esc}}(z_{\mathrm{cut}})$ curves. To reduce the effect of outliers, the mean escape time was also estimated based on the observed exits in the first 50 ns of each trajectory and correcting for those oxygens that had not yet exited by using the maximum-likelihood estimator for randomly censored data,[33,34] but this did not change the statistic conclusions in the Results and Discussion section. Likewise, the results were not affected by

considering the median of the observed exit times of a system, i.e. the average of the 20th and 21st exit of 40 exits, nor by dropping the five highest and five lowest outliers.

Finally, the extended trajectories allowed us to repeat the BA methodology several times, resulting in an estimate of the standard deviation on the BA τ, $L_{||}$ and P values (see Supp. Info. for details) for the systems at 298 K.

III. Results and Discussion

A. Times and lengths from Bayesian analysis

The Bayesian analysis of the MD trajectories provides the free energy (F) and diffusion profiles ($D_{\perp}$, $D_{||}$) across the membrane. These profiles are used to construct the matrices R', R'', $\mathcal{D}'$, and $\mathcal{D}''$ in the expressions in Table 1, yielding the characteristic times and lengths. The chosen membrane thickness is included in Table 3. The characteristic lengths show that an O_2 molecule at the surface of the membrane quickly enters the membrane and reaches the center of the membrane at $z = 0$ in 0.7 ns at 298 K and 0.4 ns at 323 K. It takes considerably longer for O_2 to escape from the center of the bilayer and to return to the water layer, because the hydrophobic region of the bilayer acts as an O_2 trap. The crossing time τ_{cross} is 15.5 ns to 32.4 ns. The crossing time is the sum of the entrance time and the escape time, so $\tau_{\text{esc}} \approx \tau_{\text{cross}}$. Trapping O_2 at the center is thus a fast process, but releasing O_2 is slow. Tracking the MD trajectories of O_2 molecules explicitly confirms this observation: O_2 spends considerable time in the tail region, and crossing the head group region is only possible for O_2 after undertaking multiple attempts to exit (see Supp. Info. of Ref. 5 for selected trajectories).

The residence time τ_{res} is shorter than the escape time τ_{esc}. The reason is that the residence time assumes the equilibrium distribution at the starting point with particles spread over the membrane and mostly located at the tail region, and two absorbing boundary conditions are assumed. The residence time is the average of how fast each of the particles can reach the membrane surface, be it at the top or at the bottom. For POPC, the residence time of 22.1 ns is higher than the 12.4 ns reported by Cordeiro et al.[35] Their value was estimated as the long-time scale decay time of a correlation function, obtained directly, without constructing the propagator, from the oxygen trajectories in NPT simulations with Gromacs using a different force field.

Oxygens move radially in the membrane over a distance $L_{||,\text{esc}}$ of 127 to 170 Å before

escaping over a normal distance of about $h/2 = 25\,\text{Å}$. The anisotropy is quantified by the ratio $L_{||,\text{esc}}/(\sqrt{2}h/2)$, where the factor $\sqrt{2}$ corrects for the 2-dimensionality of the radial diffusion versus the 1-dimensionality of the normal diffusion. The anisotropies of 3.5 to 4.7 in Table 3 show that membranes have considerably higher O_2 transport efficiency in the radial direction than in the normal direction.

Table 3: Characteristic times and lengths for oxygen diffusion in lipid bilayers calculated from two-dimensional diffusion model determined by BA of MD trajectories.[a]

	298 K	310 K			323 K		
prop	DOPC	DOPC	POPC	MITO	DOPC	POPC	DPPC
τ_{esc}	31.7	22.7	30.4	20.6	15.1	15.4	25.0
τ_{cross}	32.4	23.2	31.0	21.2	15.5	15.8	25.4
τ_{entr}	0.7	0.5	0.6	0.6	0.4	0.4	0.4
τ_{res}	30.9	22.1	29.5	19.8	14.6	15.0	24.5
h	50.7	50.2	51.6	52.9	49.6	49.4	51.7
$L_{\|\|,\text{esc}}$	145	137	150	130	127	130	170
$L_{\|\|,\text{cross}}$	147	139	151	132	129	132	172
$L_{\|\|,\text{entr}}$	14.6	15.0	13.9	15.8	15.3	14.7	14.1
anis. $\frac{L_{\|\|,\text{esc}}}{\sqrt{2}h/2}$	4.1	3.9	4.1	3.5	3.6	3.7	4.7
P	23.1	38.9	25.9	35.8	47.5	39.6	45.5
$P_{\|\|}$	32.7	41.2	35.6	39.0	53.8	54.9	55.7
$P/P_{\|\|}$	1.4	1.1	1.4	1.1	1.1	1.4	1.2

[a] Membrane thickness h (in Å), permeability P and radial permeability $P_{||}$ (in cm/s), and anisotropy ratio (no units). All times τ (in ns) and distances $L_{||}$ (in Å) are based on the F, $D_{\perp}$ and $D_{||}$ profiles obtained from BA and the expressions in Table 1. For DOPC/298, the standard deviations on τ_{esc}, $L_{||,\text{esc}}$ and P are approximately 1.1 ns, 2.5 Å, and 2.3 cm/s, respectively (see Supp. Info. for details).

A temperature increase shortens the characteristic times for the DOPC and POPC membranes drastically. Molecules exit the membrane more quickly, and consequently, $L_{||}$ is smaller. However, $L_{||}$ is less sensitive to temperature than τ. For instance, $L_{||,\text{esc}}$ decreases from 145.5 to 127.0 Å between 298 and 323 K for DOPC, while τ_{esc} decreases by a factor of two in this temperature range. $L_{||,\text{cross}}$ follows the same trend, whereas $L_{||,\text{entr}}$ slightly increases with temperature, reflecting the faster diffusion.

As the diffusivities increase with temperature, the permeabilities P in Table 3 also increase significantly. The radial permeability $P_{||}$ through a slab of thickness h, as defined in Ref. 5, shows the same behavior, but the anisotropy ratio $P/P_{||}$ varies somewhat with temperature.

A number of composition effects are evident in Table 3. O_2 moves consistently faster in the MITO membrane than in, e.g., the POPC membrane at 310 K. This reflects the combined effects of the slightly higher diffusion constant and slightly lower free energy barrier in the head group region for MITO (profiles in Ref. 5). The comparison of these two membranes shows that subtle changes in D or F affect the characteristic times considerably. Despite the similarities between the membranes, the residence time for POPC is about 50% higher than for MITO.

Oxygen diffusion is found to be faster at higher temperature (Table 3 and Ref. 22), while the solubility of oxygen in the membrane with respect to water decreases. The effect of unsaturation is apparent by comparing DPPC with two saturated chains, DOPC with two unsaturated chains, and POPC with one saturated and one unsaturated chain. As seen in earlier work, oxygen solubility in DPPC is higher than in unsaturated lipids.[22] Diffusion in saturated lipids is found to be faster at the membrane center and slower near the head group region than in unsaturated lipids. Both normal and radial diffusivities cover a larger range across the membrane at 323 K in DPPC (saturated) than in DOPC (unsaturated), whereas POPC has intermediate diffusivity (profiles in Supp. Info.).

B. Connection between P, $P_{||}$, τ, and $L_{||}$

This subsection considers the connection between permeability, characteristic times and characteristic lengths. The aim is to highlight the most relevant properties to describe permeant transport through lipid bilayers. First, let us look at the normal diffusion through the membrane, which is quantified by the permeability P and crossing time τ_{cross}. High P or low τ_{cross} are indications of efficient transport across the membrane. However, τ_{cross} cannot be used as

a direct predictor of P. This is made clear by the ratio P/τ_{cross} which varies strongly among the different lipid compositions and temperatures. The inverse $1/P$ also fails to predict τ_{cross}, as shown by the variation in the product $P\,\tau_{\text{cross}}$ in Table 4.

Table 4: Comparison of properties for normal diffusion and radial diffusion.[a]

	298 K	310 K			323 K		
	DOPC	DOPC	POPC	MITO	DOPC	POPC	DPPC
P/τ_{cross}	0.71	1.68	0.83	1.69	3.07	2.50	1.79
$P\ \tau_{\text{cross}}$	75	90	80	76	74	63	116
$P_{\|\|}/L_{\|\|,\text{cross}}$	0.22	0.30	0.23	0.29	0.42	0.42	0.32
$D_{\|\|}^{\text{ave}}$	0.169	0.213	0.184	0.201	0.278	0.284	0.288
$L_{\|\|,\text{pred}}$	148	140	151	131	131	134	171

[a] The properties are ratio P/τ_{cross} (in cm/s/ns) and product $P\ \tau_{\text{cross}}$ (in Å), ratio $P_{||}/L_{||,\text{cross}}$ (in m/s/Å), average radial diffusion coefficient $D_{||}^{\text{ave}}$ (in Å^2/ps), and predicted traveled distance $L_{||,\text{pred}}$ (in Å). All values are based on the F, $D_\perp$ and $D_{||}$ profiles obtained from BA.

To understand this non-correlation, consider the case of a high crossing time, i.e. a membrane where the permeant molecules take on average a long time to reach the other side of the membrane. This can have three reasons: (1) the diffusion coefficient of the permeant in the membrane is very low, (2) the permeant is trapped in the bilayer center in a free energy well, or (3) the permeant has to overcome a high free energy barrier while moving through the bilayer. The corresponding permeabilities for these three cases will be (1) low, (2) high, and (3) low, respectively, because the permeability incorporates the effects of the free energy profile. The permeability is modulated by the relative permeant concentrations inside and outside the membrane, while the crossing time is not. Therefore, both P and τ_{cross} are important indicators of oxygen transport through lipid membranes. When τ_{cross} is high, additional insight is given by the entrance versus escape times. They can help distinguish between permeants that are trapped in a deep free energy well, where $\tau_{\text{entr}} \ll \tau_{\text{esc}}$, and

permeants that need to overcome a high barrier $\tau_{\text{entr}} \gg \tau_{\text{esc}}$. O_2 belongs to the former situation, as evident from Table 3, and water belongs to the latter.

Second, let us look at the radial diffusion inside the membrane, which is quantified by the radial permeability $P_{||}$ and radial distance during crossing $L_{||,\text{cross}}$. High values are an indication of efficient transport inside the membrane. The ratio $P_{||}/L_{||,\text{cross}}$ in Table 4 lies in a fairly small range, with the ratio increasing consistently with temperature. The radial permeability correlates well with the radial distance, because for radial diffusion no modulation by the free energy is needed. Moreover, the average radial diffusion coefficient $D_{||}^{\text{ave}}$ is computed (see Ref. 5), and Table 4 shows that the radial transport is fairly equally efficient among the different membranes compositions at a given temperature.

Next, the $D_{||}^{\text{ave}}$ value is used to predict the average traveled squared distance in the time that the O_2 spends in the membrane,

$$L_{||,\text{pred}}^2 = 4D_{||}^{\text{ave}}\tau_{\text{cross}}. \tag{29}$$

The resemblance between this prediction in Table 4 and $L_{||,\text{cross}}$ in Table 3 is striking. It means that the diffusion inside the membrane parallel to the surface is indeed well described by two-dimensional diffusion with diffusivity $D_{||}^{\text{ave}}$. The traveled lengths during escape/crossing/entrance of the permeant are based on the same average diffusivity, and differences between those three lengths are therefore mostly explained by the different considered times associated with escape/crossing/entrance. Note, however, that, in general, the r-dependence of the propagator is not simply Gaussian, even though the free energy is independent of r. The reason is that through the z-dependence of $D_{||}(z)$, different trajectories accumulate different variances in r. Eq. 29 is hence only a good approximation for long time scales.

In conclusion, several properties have been derived from the F, $D_{\perp}$ and $D_{||}$ profiles to quantify the transport. From a list of the properties considered in this work, the most

relevant descriptors are: h, P, τ_{cross} (or τ_{esc}), τ_{entr}, and $L_{||,\mathrm{cross}}$ (or $D_{||}^{\mathrm{ave}}$). The combination of these descriptors provides a picture of permeant diffusion through the membrane. For instance, MITO has higher transport efficiency in the radial direction than POPC at 310 K, which translates itself mostly in higher P and shorter τ_{cross}. The membranes are similar for τ_{entr} and for radial transport, as can be seen in $L_{||,\mathrm{cross}}$.

Note that other methods can be used to determine permeability. Permeant transport through the membrane has been determined directly from the flux by counting the rate of membrane escape events in equilibrium simulations.[36] In explicit gas diffusion simulations, oxygens are placed in the bulk water phase in the beginning of the simulation, and in induced pressure simulations, oxygen molecules are given a constant force along the normal.[37,38] For permeants with sufficiently high membrane crossing rates, permeation can be obtained by measuring crossing times with milestoning.[39] A rough estimate for permeation of NH_3 and CO_2 through pores was obtained by multiplying a constant diffusivity with an Arrhenius factor containing the free energy barrier.[40,41] The important advantage of the present work is that the BA approach based on the Smoluchowski equation not only provides the permeability but also all of the above mentioned properties in Table 3-4, giving a more complete picture.

C. Comparison of BA with direct observation in trajectories

The Bayesian approach using the profiles has as an additional practical advantage that shorter trajectories may be used to gather data, in our case 50 ns per replicate. In principle, many even shorter trajectories could be collected to perform the Bayesian analysis. This is in stark contrast to the direct observation of exit times, where long trajectories are required to observe an exit of all of the oxygens. An important question is thus whether the Bayesian analysis successfully reproduces the exits observed in the trajectories. To answer this question, the MD trajectories have been extended until each of the 10 oxygens in each of the 4 replicates exited the membrane at least once, requiring up to 297 ns for the slowest oxygen.

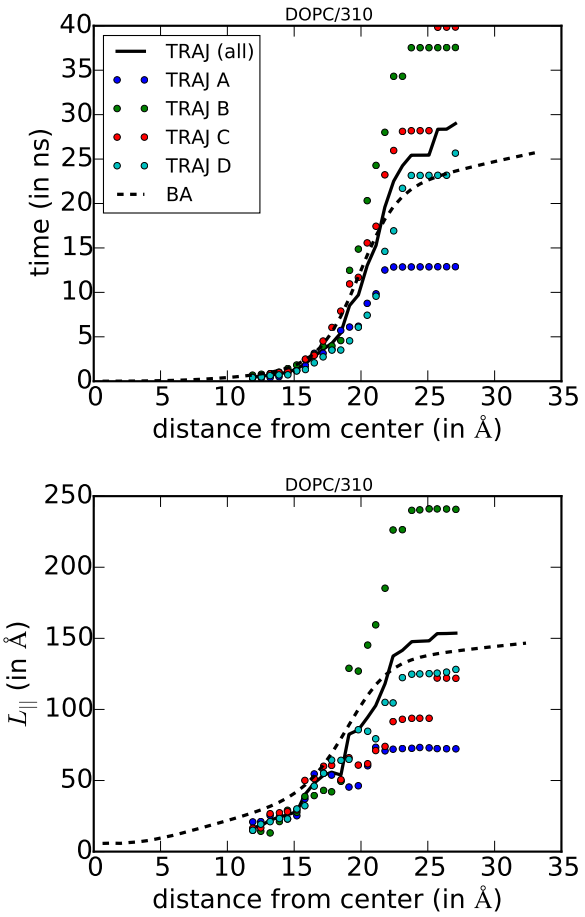

Figure 4: (Top) Escape time $\tau_{\rm esc}(z_{\rm cut})$ and (bottom) traveled radial distance $L_{||,{\rm esc}}(z_{\rm cut})$ for DOPC/310 bilayer as a function of half the thickness $z_{\rm cut}$ of the considered slab. The surface of the membrane is located at $h/2 \approx 25$Å. The Bayesian prediction (dashed line) is compared to the average of 10 oxygens as observed in the four MD replicates A/B/C/D (colored dots) and the average of all 40 observed exits (solid line).

Fig. 4 compares Bayesian analysis (BA) and direct observations in trajectories (TRAJ) for DOPC/310. It shows the escape time $\tau_{\rm esc}(z_{\rm cut})$ and traveled radial distance $L_{||,{\rm esc}}(z_{\rm cut})$ curves for a series of slab thicknesses. The curves are widely spread, indicating that escape times and lengths have a wide distribution with slowly converging statistics. Fig. 5 combines all seven investigated systems, again covering a series of slab thicknesses. The membrane thickness is indicated with a square at $h/2 \approx 25\,$Å. A perfect correspondence between BA and TRAJ would place all curves on the diagonal of Fig. 5. In most of the systems, the BA overestimates $\tau_{\rm esc}(z_{\rm cut})$ inside the membrane (bottom left corner), and underestimates it

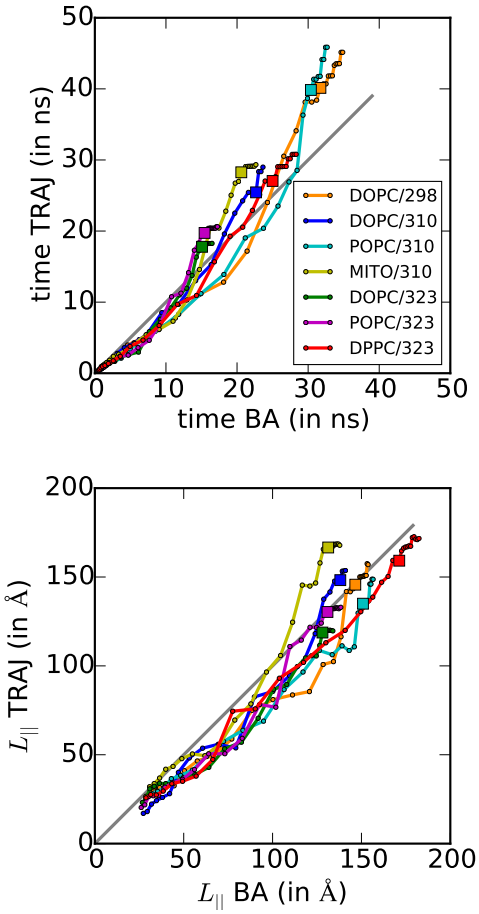

Figure 5: (Top) Scatter plots of the results from MD simulation and the two-dimensional diffusion model for the escape times $\tau_{\mathrm{esc}}(z_{\mathrm{cut}})$ and (bottom) traveled radial distance $L_{||,\mathrm{esc}}(z_{\mathrm{cut}})$ for all seven bilayers. Each dot represents the result obtained for a slab with half thickness z_{cut} ranging from 12 Å to approximately 27 Å (individual curves in Supp. Info.). The Bayesian prediction (x-axis) is compared to the average of all 40 observed exits (y-axis). The escape from a slab with membrane thickness h is indicated with a square.

when z_{cut} is at the membrane/water interface and beyond (top right corner). The traveled radial distance $L_{||,\mathrm{esc}}(z_{\mathrm{cut}})$ is also overestimated by BA inside the membrane, but agrees with the TRAJ value (on average) at the membrane/water interface.

Next, we wish to quantify the difference between BA and TRAJ for the escapes from the membrane ($z_{\mathrm{cut}} = h/2$). However, escape times have notoriously poor statistics. An analogy can be made to the waiting time of a Poisson process. The standard deviation of the waiting time distribution, $P(t) \sim e^{-t/T}$, is equal to the mean itself, T. Hence a relative standard error of 10% would require roughly 100 observations, and this would give a fairly wide 95%

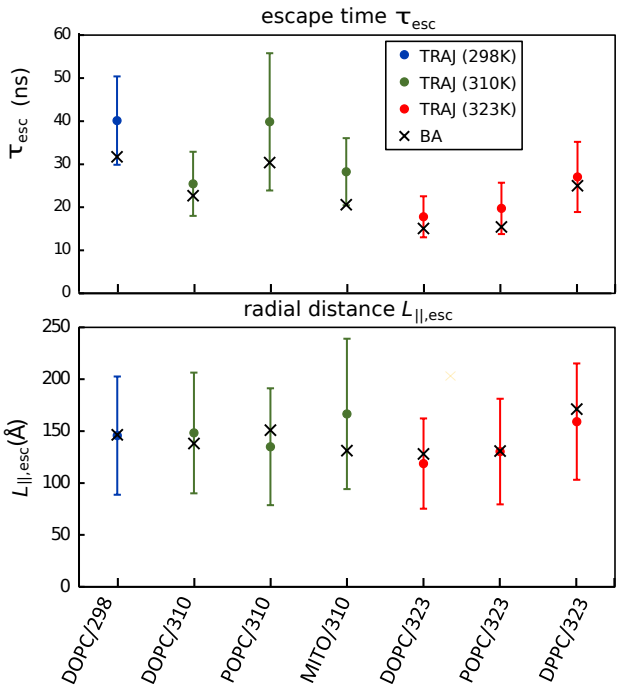

Figure 6: (Top) Escape time $\tau_{\rm esc}$ and (bottom) traveled radial distance $L_{||,\rm esc}$ for all seven bilayers, for membrane thickness h (for $z_{\rm cut} = h/2 \approx 25\,$Å). The Bayesian prediction (BA, cross) is compared to the average of 40 observed exits with indication of its 95% confidence interval (TRAJ, dot).

confidence interval of ±20% for the mean waiting time. Likewise, the confidence interval provided by 40 observed exits would be about ±30%, and this shows that the statistics provided by the 40 O_2 exits are not sufficient to quantify the difference between BA and TRAJ if it is smaller than ±30%.

In Fig. 6, the value from BA is bracketed by the 95% confidence interval of TRAJ for each system, indicating that the difference is not statistically significant on a per-system basis. However, the deviation BA < TRAJ for $\tau_{\rm esc}$ is systematic over the seven systems, and pooling the systems yields a test with higher power. The aggregate of the seven systems contains 280 observed exits, and this number is high enough to yield a statistically significant difference. The average of 40 observed exits for each system can be assumed to be normally distributed. A paired test with unknown variances was performed on the 7 systems between $\tau_{\rm esc}^{\rm TRAJ}$ and $\tau_{\rm esc}^{\rm BA}$, giving a t-value of 4.6 with p-value 0.0038. This allows us to conclude that the BA

systematically underestimates the TRAJ escape time, and that the underestimation is 7 to 27%. Consequently, BA permeabilities can be expected to suffer from an overestimation in a similar percentage range. Whether this inaccuracy associated with the BA is acceptable or not depends on the application. When very accurate escape times are required, one can follow the straightforward approach based on registering exits from very long trajectories and multiple replica systems. Note that four replicates totalling 40 observed exits still give a large confidence interval in Fig. 6, so more replicates would be needed to estimate a statistically more precise result than the BA approach. This inaccuracy inherent in the BA approach is smaller than the 30% error found in experimental permeabilities.[42] When experimental accuracy is sufficient, the BA approach is a valid and computationally attractive alternative to TRAJ.

For $L_{||,\mathrm{esc}}$, the paired test gives a t-value of 0.15 with p-value 0.89. Based on the 280 observed exits, the BA and TRAJ radial traveled distance do not differ significantly. Lastly, the precision of the BA was determined for the DOPC membranes at 298 K by repeating the BA several times (see Section V.B in Supp. Info. for a detailed analysis). The % errors, evaluated as the standard deviation divided by the mean, for DOPC/298 are 3% for τ_{esc} and 2% for $L_{||,\mathrm{esc}}$. These errors on τ_{esc} and $L_{||,\mathrm{esc}}$ based on 50 ns trajectories (see Section II.C) are substantially smaller than those of the TRAJ values (Fig. 6) based on the long extended trajectories. This statistical analysis shows the added value of constructing the theoretical propagators with Bayesian analysis and deriving times and lengths, as proposed in this paper: escapes from the membrane take place on the long time scale, but the distances traveled can nevertheless be predicted without simulating very long trajectories.

The underlying assumption in the Bayesian analysis is that the kinetics of oxygen transport are described by the Smoluchowski equation. The transport is assumed to be diffusive, without memory effects of the solvent (here the lipid and water molecules). In contrast to BA, the TRAJ times and lengths are 'pure' observations and do not assume a diffusive model. The deviations for τ_{esc} between BA and TRAJ, while relatively small, are likely rooted in

the Smoluchowski equation failing to describe the oxygen transport kinetics. Several points can be made about this.

The dynamics of oxygen molecules is indeed not purely diffusive, not even in neat water or in neat hexadecane, a model for the lipid tails. In realistic systems diffusive behavior should be regarded as a phenomenological law; at the shortest time scales the behavior is ballistic, and it is only at slightly larger time scales that diffusive behavior might set in. In the specific case of O_2 in water, hexadecane, or lipids, an additional transient regime was noticed for lag times up to 20 ps in Ref. 5. The initial slope of the MSD was higher, giving a higher diffusivity at the short time scale, which can be interpreted as fast rattling motions within free volume pockets. After a lag time of 20 ps, the diffusive regime was reached with a constant diffusivity, whose motions can be interpreted as jumps between pockets. The BA was repeated using various lag times, and a fit of the slope allowing for an offset was done to reach this diffusive regime, as specified in the Theory and Methods section. The characteristic times and lengths are however computed with the propagator p, disregarding the transient regime altogether. At the time scale of crossing the membrane, which is 16 to 32 ns, this transient regime of 20 ps is negligible for the τ and $L_{||}$ predictions, and cannot be the source for the deviations in τ_{esc}.

Another route of thought is the role of inhomogeneity. Oxygen crossing over the free energy barrier in the head group region is a fast process, during which oxygen might receive insufficient collisions to randomize the forces by the solvent. In this scenario, memory starts playing a role. The advanced approaches mentioned in the Introduction assume increasingly more complicated mathematical models at the origin of the dynamics, e.g. by including memory kernels, to match the observations in MD. It is likely that some of the deviations between BA and TRAJ can be accounted for in a model that includes memory effects. Non-diffusive effects could be responsible for the underestimation of τ_{esc} by 7-27%, as normal transport suffers from the inhomogeneities with free energy barriers and wells, where oxygen rolling off a barrier could imply a memory effect. Meanwhile, $L_{||,\mathrm{esc}}$ would not be significantly

affected, as the free energy is constant for radial transport, and the two-dimensional radial MSD of oxygen indeed grows linearly in time in MITO/310 and POPC/310 (see Ref. 5). Overall, the diffusive picture implied by the Smoluchowski equation is found here to give a sufficiently accurate estimation of the O_2 dynamics for the modeled membranes, even without resorting to more advanced mathematical models.

Yet another limitation of the Smoluchowski equation could be the dimensionality. The diffusive coordinate is the position of oxygen with respect to the membrane center $z = 0$. Local fluctuations of the environment are not taken into account, such as membrane undulations or lipid protrusions. Membrane undulations displace the membrane center locally, while lipid protrusion causes roughness at the bilayer/water interface. As a result, the instantaneous position of any atom in the head group may differ substantially from the average position of all of the head groups. Hence, the path taken by a particular oxygen as it crosses this interface might be not well represented by the free energy and diffusion profiles obtained from the BA. The next subsection discusses the effect of undulations on the Smoluchowski equation.

D. Effects of membrane undulations

Membrane undulations are affected by the simulation box size. The bilayers presented so far are small (72 lipids). While these systems exhibit some local roughness with lipid protrusions or tilts, they are globally flat on the 5 nm length scale of the simulation cell. As the system size increases, longer wavelength undulations of the membrane must be considered.[43,44] As an example, Fig. 7 compares $F(z)$ and $D(z)$ for a DOPC bilayer consisting of 288 lipids (10 nm on a side) and the 72 lipid DOPC bilayer (5 nm side) already discussed. These BA profiles lead to $\tau_{\mathrm{esc}}^{\mathrm{BA}} = 24.2$ ns for the 288 lipid system, which is substantially lower than the value of 31.7 ns for the 72 lipid system (Table 5). The relative standard deviation on these escape times is estimated to be 3% (see Supp. Info.). Oxygen apparently escapes faster in the larger simulation box according to the BA values.

The faster escape for the large system can be explained by the increased membrane roughness. The larger simulation box allows for larger amplitudes of membrane undulations, which causes the z-coordinate to become a less accurate descriptor. The z-axis is the position of oxygen with respect to the membrane center of all lipids, without taking into account local fluctuations in membrane thickness or of the membrane center, and assuming that the bilayer normal is coincident with the z-axis in the lab frame. The membrane undulations play the role of hidden variables for the free energy and dynamics,[45] and F barriers may therefore be underestimated. This is confirmed in Fig. 7, where the large system's F profile has less sharp features. The details are washed out by the fluctuations, giving a less deep free energy well with respect to the water phase and a lower free energy barrier than for the small simulation box. Similar effects have been found when comparing electron density profiles from simulations of large systems with those extracted from experiment.[46–48]

Table 5: Comparison of times and lengths for DOPC at 298 K between the small (DOPC/298) and large (DOPC/298/lg) simulation box.[a]

		BA			TRAJ		
	z_{cut} (Å)	DOPC/298	DOPC/298/lg	diff.	DOPC/298	DOPC/298/lg	diff.
$\tau_{\mathrm{esc}}(z_{\mathrm{cut}})$	25	31.7	24.2	24%	40 ± 10	35 ± 9	13%
	32	34.9	27.2	22%	45 ± 11	42 ± 10	7%
$L_{\|\|,\mathrm{esc}}(z_{\mathrm{cut}})$	25	146	120	18%	146 ± 57	106 ± 36	27%
	32	153	127	17%	157 ± 60	146 ± 65	7%

[a] Escape times τ (in ns) and lengths (in Å) are evaluated for a slab with half thickness $z_{\mathrm{cut}} = h/2$, as in Table 3 (25.4 and 25.1 Å for small and large box, respectively). The larger half thickness $z_{\mathrm{cut}} \approx 32$ Å puts the dividing surface in the water phase (32.7 and 32.4 Å for small and large box, respectively). Diff. refers to the difference relative to the small box value. The standard deviations on the BA values of τ_{esc} and $L_{||,\mathrm{esc}}$ are approximately 1.1 ns and 2.5 Å, respectively, for DOPC/298, and they are approximately 0.6 ns and 1.5 Å for DOPC/298/lg (see Supp. Info. for details). The uncertainty intervals for the TRAJ values are for the 95% confidence intervals.

The free energy is clearly the average over a dynamic surface with roughness caused by undulations and lipid protrusions. This information is absent in the Smoluchowski model for the membrane, as it treats the membrane as an inhomogeneous yet static medium. The one-

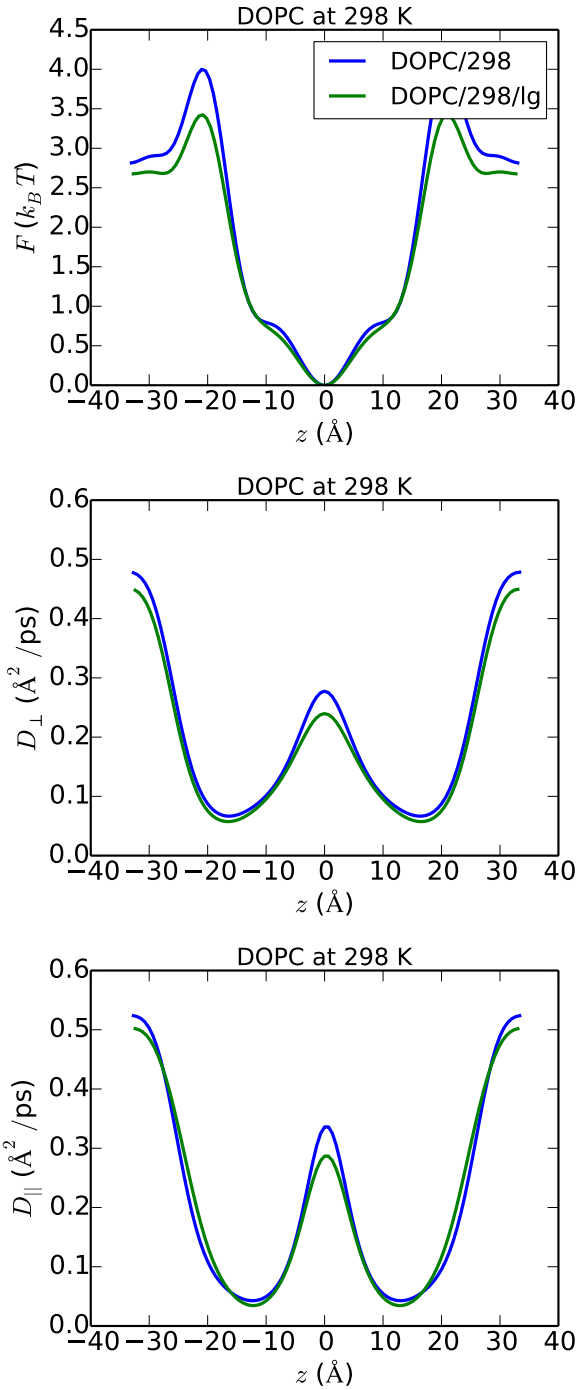

Figure 7: Comparison of DOPC free energy (top) and diffusion profiles (center, bottom) at 298 K obtained by BA of simulations with boxes of 72 lipids (DOPC/298) and 288 lipids (DOPC/298/lg).

dimensional $F(z)$ convolutes the local free energy with fluctuations in the membrane. The Smoluchowski model quality suffers under the hidden variables (roughness). The smaller

systems are less sensitive for these undulations, and therefore the BA can be used with confidence for bilayers on the 5 nm length scale. In larger membranes, a correction should be applied to remove the effect of undulations, such as the Fourier-based corrections proposed for electron density calculations.[49,50] In essence, the correction determines the local membrane center and lipid tilt, and updates the oxygen position to a local reference frame.

In the trajectories, the TRAJ value obtained by observing 40 escapes is $\tau_{\mathrm{esc}}^{\mathrm{TRAJ}} = 35 \pm 9$ ns for the large system and 40 ± 10 ns for the small system, where the errors refer to the 95% confidence intervals associated with the 40 observations. The TRAJ values follow the same trend as the BA, with faster oxygen exits in the large than in the small system. However, $\tau_{\mathrm{esc}}^{\mathrm{TRAJ}}$ for the large box is statistically equivalent to $\tau_{\mathrm{esc}}^{\mathrm{TRAJ}}$ for the smaller box, as determined by an unpaired t-test with p-value 0.42 (see Supp. Info.).

The TRAJ escape times are also based on the same single coordinate z to detect the exits and will hence also be affected by membrane undulations. However, the BA and TRAJ approaches are different in nature. BA uses the MD data to extract the Smoluchowski model parameters for the transport kinetics, whereas TRAJ directly measures τ in a model-free way. This major difference between model versus model-free approach leads us to expect that TRAJ is less sensitive to membrane roughness than BA. The current data in Table 5 are not sufficiently precise to confirm this with statistical significance, but nevertheless support the expected trend with a box size effect of 13% for TRAJ and 24% for BA. Moreover, a larger slab was considered by increasing z_{cut} to 32 Å, which puts the dividing surface completely in the water phase. For the TRAJ escape times, the membrane undulations have less effect further away from the membrane, leading to a reduced box size effect of only 7% (however not statistically relevant). In contrast, this larger slab fails to reduce the BA box size effect, because the Smoluchowski model in BA does not change at all by considering a different dividing surface.

The $L_{||,\mathrm{esc}}$ values decrease in the larger system, which is mostly explained by the shorter time spent in the membrane. The radial transport is thus fairly similar in the 72 and 288

lipids. This can be expected because the O_2 spends most of its time trapped in the lipid region, and its radial dynamics are less affected by undulations. The TRAJ values are again statistically equivalent for the large and small system (see Supp. Info.) with a p-value of 0.079.

IV. Conclusion

A central question for oxygen transport is the balance between normal and radial transport in phospholipid membranes because of its importance for biological function. Based on the Smoluchowski equation for inhomogeneous diffusion, Bayesian analysis (BA) can be applied to MD trajectories of oxygen to extract the free energy, the normal diffusion and the radial diffusion profiles. The propagator is two-dimensional, depending not only on the normal coordinate z but also on the radial coordinate r. In a two-dimensional treatment, formulas (Eqs. 10, 17, 28, and 25) can be given for the average times as well as average radial distances associated with entering, escaping, or crossing the membrane. The formalism is based on mean first passage times and holds for any process described by rate equations between discrete states, i.e. of the type in Eq. 3, and therefore it can be expected that our approach can be used for other geometries, e.g. where the medium is not necessarily a layered membrane, or where source and sink terms are present for the permeants.

Eight model membranes with varying lipid composition and temperature were simulated. In the time needed to cross the membrane, which is on average about 16 to 32 ns, the oxygen molecule travels about 3.5 to 4.7 times further in the radial than in the normal direction. This finding confirms the proposition that O_2 is trapped in the bilayer and has time to diffuse radially, as it takes a significant time to diffuse out of the bilayer.

The connection between permeabilities, crossing times, and traveled radial lengths is discussed, and it is shown how each property contributes additional insight in the transport process. The most relevant properties for developing a model of normal and radial permeant

diffusion in cell membranes are h, P, τ_{cross} (or τ_{esc}), τ_{entr}, and $L_{||,\text{cross}}$ (or $D_{||}^{\text{ave}}$). While simulations of protein-containing bilayers are required to support and refine the model, the present simulations indicate that oxygen quickly enters the membrane and proceeds to the interleaflet space. It then has ample time (15-32 ns) to diffuse radially over 127 to 170 Å. The mismatch of normal and radial diffusive lengths allows oxygen to interact with membrane proteins containing binding pockets in the center of the membrane, such as cytochrome c oxidase.[51,52]

The preceding times and distances based on the Bayesian analysis approach were compared with an aggregate of 280 membrane exits explicitly observed in extended simulated trajectories. This provides a direct test of the BA approach and the applicability of the Smoluchowski equation to membrane diffusion. While the statistical error of quantities related to first passage times from individual MD simulations is high, the aggregate of 280 exits (7 systems, 4 replicates, 10 oxygens) is sufficient to provide reasonable level of confidence. Specifically, the BA underestimates O_2 escape times by approximately 20%, corresponding to a near negligible difference in the effective barrier at the water/membrane interface. There is no statistically significant difference for the radial distances, as radial transport is not subject to a free energy barrier.

Longer wavelength undulations emerging with increased system size degrade the performance of the BA as it is currently implemented. For a larger box size, a correction should be applied to determine the O_2 position with respect to the local membrane center. Fortunately, membrane undulations have a very small effect for smaller simulation boxes, such as the 5 nm systems presented here. Consequently, escape times and permeabilities should be directly comparable to experiment.

In closing, the Bayesian Analysis introduced in Ref. 5 and further developed in this paper is a computationally attractive method for estimating characteristic times, permeability, and radial distances for permeants from simulations of lipid bilayers. It is precise, in that trajectories can be much shorter than would be required to obtain the preceding

quantities directly from MD trajectories and with comparable statistical uncertainty. It is also sufficiently accurate for most applications, in that characteristic times for oxygen are within approximately 20% of simulation, and radial distances are statistically indistinguishable. Though presently only tested for oxygen, the preceding comparisons strongly support the use of the Smoluchowski equation and the inhomogeneous solubility-diffusion model to describe passive transport of permeants in membranes. The new methodology supports both a more detailed characterization of permeant properties and the development of detailed kinetic models of normal and radial diffusion in highly complex, inhomogeneous, and anisotropic environments.

Acknowledgement

We would like to acknowledge helpful discussions with Attila Szabo. This work was supported by the Fund for Scientific Research - Flanders (FWO), the research Board of Ghent University, the Max Planck Society, and the Intramural Research Program of the NIH, National Heart, Lung and Blood Institute. High-performance computational resources and services were provided by the National Institutes of Health, Bethesda, MD (NHLBI LoBoS cluster) and by Ghent University (Stevin Supercomputer Infrastructure).

Supporting Information Available

Supporting information: Appendix: analytical integration over r in characteristic lengths, additional information about MD runs and box sizes, comparison of $\tau(z_{\text{cut}})$ and $L_{||}(z_{\text{cut}})$ curves between BA and TRAJ for each system, precision of BA profiles, BA times and BA lengths, and error analysis for differences between DOPC/298 and DOPC/298/lg.

This material is available free of charge via the Internet at `http://pubs.acs.org/`.

References

(1) Missner, A.; Pohl, P. *ChemPhysChem* **2009**, *10*, 1405–1414.

(2) Marrink, S.; Berendsen, H. J. C. *J. Phys. Chem.* **1994**, *98*, 4155–4168.

(3) Marrink, S.; Berendsen, H. J. C. *J. Phys. Chem.* **1996**, *100*, 16729–16738.

(4) Riahi, S.; Rowley, C. N. *J. Am. Chem. Soc.* **2014**, *136*, 15111–15113.

(5) Ghysels, A.; Venable, R. M.; Pastor, R. W.; Hummer, G. *J. Chem. Theory Comput.* **2017**, *13*, 2962–2976.

(6) Chipot, C.; Comer, J. *Sci. Rep.* **2016**, 35913.

(7) Parisio, G.; Stocchero, M.; Ferrarini, A. *J. Chem. Theory Comput.* **2013**, *9*, 5236–5246.

(8) Metzler, R.; Klafter, J. *Phys. Rep.* **2000**, *339*, 1–77.

(9) Metzler, R.; Jeon, J.; Cherstvy, A. G.; Barkai, E. *Phys. Chem. Chem. Phys.* **2014**, *16*, 24128–24164.

(10) Meroz, Y.; Sokolov, I. M.; Klafter, J. *Phys. Rev. Lett.* **2013**, *110*, 1–4.

(11) Cherstvy, A. G.; Metzler, R. *Phys. Chem. Chem. Phys.* **2016**, *18*, 23840–23852.

(12) Chubynsky, M. V.; Slater, G. W. *Phys. Rev. Lett.* **2014**, *113*, 1–5.

(13) Jain, R.; Sebastian, K. L. *J. Phys. Chem. B* **2016**, *120*, 3988–3992.

(14) Gajda, J.; Mydlarczyk, W. *Phys. A* **2016**, *447*, 149–160.

(15) Chechkin, A. V.; Seno, F.; Metzler, R.; Sokolov, I. M. *Phys. Rev. X* **2017**, *7*, 1–20.

(16) Krapf, D.; Campagnola, G.; Nepal, K.; Peersen, O. B. *Phys. Chem. Chem. Phys.* **2016**, *18*, 12633–12641.

(17) Bazzani, A.; Bassi, G.; Turchetti, G. *Phys. A Stat. Mech. its Appl.* **2003**, *324*, 530–550.

(18) Jeon, J. H.; Metzler, R. *Phys. Rev. E* **2010**, *81*, 1–11.

(19) Darve, E.; Solomon, J.; Kia, A. *PNAS* **2009**, *106*, 10884–10889.

(20) Hinsen, K.; Kneller, G. R. *J. Chem. Phys.* **2016**, *145*.

(21) Hummer, G. *New J. Phys.* **2005**, *7*, 34.

(22) De Vos, O.; Van Hecke, T.; Ghysels, A. *Adv. Exp. Med. Bio.* **2018**, *submitted*.

(23) Ovchinnikov, V.; Nam, K.; Karplus, M. *J. Phys. Chem. B* **2017**,

(24) Lee, C. T.; Comer, J.; Herndon, C.; Leung, N.; Pavlova, A.; Swift, R. V.; Tung, C.; Rowley, C. N.; Amaro, R. E.; Chipot, C.; Wang, Y.; Gumbart, J. C. *J. Chem. Inf. Model.* **2016**, *56*, 721–733.

(25) Shinoda, W.; Mikami, M.; Baba, T.; Hato, M. *J. Phys. Chem. B* **2004**, *108*, 9346–9356.

(26) Rui, H.; Lee, K. I.; Pastor, R. W.; Im, W. *Biophys. J.* **2011**, *100*, 602–610.

(27) Issack, B. B.; Peslherbe, G. H. *J. Phys. Chem. B* **2015**, *119*, 9391–9400.

(28) Szabo, A.; Schulten, K.; Schulten, Z. *J. Chem. Phys.* **1980**, *72*, 4350–4357.

(29) Hänggi, P.; Talkner, P.; Brokovec, M. *Rev. Mod. Phys.* **1990**, *62*, 251–341.

(30) Venable, R. M.; Hatcher, E.; Guvench, O.; MacKerell, A. D.; Pastor, R. W. *J. Phys. Chem. B* **2010**, *114*, 12501–12507.

(31) Klauda, J. B.; Venable, R. M.; Freites, J. A.; O'Connor, J. W.; Tobias, D. J.; Mondragon-Ramirez, C.; Vorobyov, I.; MacKerell, J., A. D.; Pastor, R. W. *J. Phys. Chem. B* **2010**, *114*, 7830–7843.

(32) Brooks, B. R. et al. *J. Comput. Chem.* **2009**, *30*, 1545–1614.

(33) Yeh, I. C.; Hummer, G. *Proc. Natl. Acad. Sci. U.S.A.* **2004**, *101*, 12177–12182.

(34) Hummer, G.; Szabo, A. In *Theory and evaluation of single-molecule signals*; Barkai, E., Brown, F., Orrit, M., Yang, H., Eds.; World Scientific, 2008; pp 139–180.

(35) Cordeiro, R. M. *Biochim. Biophys. Acta - Biomembr.* **2014**, *1838*, 438–444.

(36) Dotson, R. J.; Smith, K., Bueche; Angles, G.; Pias, S. C. *Biophys. J.* **2017**, 2336–2347.

(37) Wang, Y.; Cohen, J.; Boron, W. F.; Schulten, K.; Tajkhorshid, E. *J. Struct. Biol.* **2007**, *157*, 534–544.

(38) Wang, Y.; Ohkubo, Y. Z.; Tajkhorshid, E. *Curr. Top. Membr.* **2008**, *60*, 343–367.

(39) Votapka, L. W.; Lee, C. T.; Amaro, R. E. *J. Phys. Chem. B* **2016**, *120*, 8606–8616.

(40) Hub, J. S.; de Groot, B. L. *Biophys. J.* **2006**, *91*, 842–848.

(41) Hub, J. S.; Winkler, F. K.; Merrick, M.; De Groot, B. L. *J. Am. Chem. Soc.* **2010**, *132*, 13251–13263.

(42) Widomska, J.; Raguz, M.; Subczynski, W. K. *BBA - Biomembranes* **2007**, *1768*, 2635–2645.

(43) Watson, M. C.; Penev, E. S.; Welch, P. M.; Brown, F. L. *J. Chem. Phys.* **2011**, *135*.

(44) Watson, M. C.; Brandt, E. G.; Welch, P. M.; Brown, F. L. H. *Phys. Rev. Lett.* **2012**, *109*, 1–5.

(45) Neale, C.; Pomès, R. *Biochim. Biophys. Acta - Biomembr.* **2016**, *1858*, 2539–2548.

(46) Braun, A. R.; Brandt, E. G.; Edholm, O.; Nagle, J. F.; Sachs, J. N. *Biophys. J.* **2011**, *100*, 2112–2120.

(47) Braun, A. R.; Sachs, J. N. *Annu. Rep. Comput. Chem.*; Elsevier B.V., 2011; Vol. 7; pp 125–150.

(48) Brandt, E. G.; Braun, A. R.; Sachs, J. N.; Nagle, J. F.; Edholm, O. *Biophys. J.* **2011**, *100*, 2104–2111.

(49) Albert, J. C.; Ray, L. T.; Nagle, J. F. *J. Chem. Phys.* **2014**, *141*.

(50) Gapsys, V.; de Groot, B. L.; Briones, R. *J. Comput. Aided. Mol. Des.* **2013**, *27*, 845–858.

(51) Riistama, S.; Puustinen, A.; García-Horsman, A.; Iwata, S.; Michel, H.; Wikström, M. *Biochim. Biophys. Acta* **1996**, *1-4*.

(52) Wikström, M.; Sharma, V.; Kaila, V.; Hosler, J.; Hummer, G. *Chem. Rev.* **2015**, *115*, 2196–2221.

Table of Contents Figure

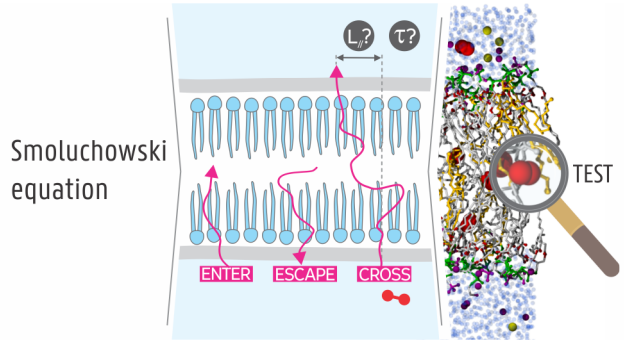

Figure 8: TOC